Title

In vivo perturb-seq of cancer and immune cells dissects oncologic drivers and therapy response

Author List

S. John Liu[1,2,3], Joanna Pak[1,2,5], Christopher Zou[1,2], Timothy Casey-Clyde[1,2,5], Ashir A. Borah[3,4], David Wu[2], Kyounghee Seo[1,2,5], Thomas O'Loughlin[8], Daniel A. Lim[2], Tomoko Ozawa[2], Mitchel S. Berger[2], William A. Weiss[2,6], David R. Raleigh[1,2,5]*, Luke A. Gilbert[3,7]*

*Equal contribution

[#]Correspondence: luke@arcinstitute.org and david.raleigh@ucsf.edu

Affiliations

[1]Department of Radiation Oncology, University of California San Francisco, San Francisco, CA 94143, USA

[2]Department of Neurological Surgery, University of California San Francisco, San Francisco, CA 94143, USA

[3]Arc Institute, Palo Alto, CA 94304, USA

[4]Biological and Medical Informatics Graduate Program, University of California San Francisco, San Francisco, CA 94143, USA

[5]Department of Pathology, University of California San Francisco, San Francisco, CA 94143, USA

[6]Departments of Pediatrics, Neurology, and Helen Diller Family Comprehensive Cancer Center, University of California, San Francisco, CA 94143, USA

[7]Department of Urology, University of California San Francisco, San Francisco, CA 94143, USA

[8]Department of Neuroscience, Icahn School of Medicine, Mount Sinai, New York, NY 10029, USA

Abstract

Genetic perturbation screens with single cell readouts have enabled rich phenotyping of gene function and regulatory networks. These approaches have been challenging *in vivo,* especially in adult disease models such as cancer, which include mixtures of malignant and microenvironment cells. Here, we develop a multiplex *in vivo* perturb-seq CRISPRi platform for single cell genetic screens in cancer and immune cells that leverages intracranial convection enhanced delivery of sgRNA libraries into models of glioblastoma (GBM), a fatal brain cancer. Our results reveal *in vivo* specific rewiring of genetic dependencies in response to radiotherapy, a potent yet non-curative therapy for GBM, as well as alterations of ligand-receptor interactions between microenvironment cells. In sum, we demonstrate the utility of multiplexed perturb-seq for *in vivo* single cell dissection of adult tissue biology across multiple cell types in the context of therapeutic stimuli.

Main

Functional understanding of genes under physiological and disease states *in vivo* has been limited by a lack of approaches for multiplexed genetic perturbation at single cell resolution. CRISPR functional genomics have transformed our understanding of how genetic and epigenetic perturbations impact cell types and cell states, but the majority of such efforts have focused on gene function *in vitro*[1] or utilize *ex vivo* perturbations[2,3]. *In vivo* functional genomics approaches have largely focused on population averaged phenotypes, obscuring cellular heterogeneity and cell-cell interactions that are critical for multicellular biology, disease, and response to stimuli. Here we test the hypothesis that perturb-seq, which couples single cell RNA-sequencing (scRNA-seq) with CRISPR perturbations[4–9], enables high dimensional *in vivo* phenotyping of gene function at single cell resolution across multiple cell types in adult tissue. To establish an *in vivo* perturb-seq platform for multiplex interrogation of diseased or normal cells, we focused on glioblastoma (GBM), the most common malignant brain tumor in adults[10]. GBM is incurable and is associated with dynamic malignant cell states and numerous microenvironment cell types[11]. While multiplex *in vivo* perturb-seq has been implemented in the developing mouse brain[12], direct perturbation of malignant and microenvironment cells in tumors and more broadly in adult tissues have been hindered by limited capacity for delivery of CRISPR components *in vivo*. To address this limitation in approaches for multiplexed genetic perturbation at single cell resolution, we developed a platform for *in vivo* perturb-seq in malignant and immune cells in the tumor microenvironment using convection enhanced delivery (CED), a technique that exploits bulk flow kinetics for enhanced delivery of viral vectors[13,14]. We show that in comparison to perturb-seq performed *in vitro* or using sgRNAs delivered to GBM cells prior to *in vivo* tumorigenesis (pre-infected), CED perturb-seq uniquely reveals how therapy of established tumors

rewires transcriptional responses to genetic perturbations. This platform allows for interrogation of cellular interactions in the tumor microenvironment, highlighting the utility of perturbing cells in their intact environment.

To establish *in vivo* perturb-seq in tumor models, we transplanted syngeneic mouse GL261 GBM cells stably expressing CRISPRi (dCas9-KRAB) into the striata of C57BL/6 mice (Fig. 1A). Following tumor establishment, lentiviral dual-sgRNA libraries[15] targeting 48 genes that were nominated from *in vitro* CRISPRi growth or radiation modifier screens (Supplementary Fig. 1 and Supplementary Table 1) plus non-targeting sgRNA controls were delivered to intracranial tumors using CED. Animals were treated with either fractionated radiotherapy capable of prolonging survival but not curing *in vivo* models (RT, 2 Gy x 5 daily fractions) or no treatment (Supplementary Fig 1A). Tumors were then microdissected, dissociated, sorted for sgRNA+ cells, and harvested for scRNA-seq with direct capture of sgRNA tags[5]. To compare *in vivo* perturbations to *in vitro* perturbations, we also used perturb-seq to profile the same gene perturbations in GL261 cells *in vitro* or in GL261 cells that were transduced with sgRNA libraries prior to *in vivo* tumorigenesis (pre-infected) (Fig. 1A). Integrated scRNA-seq of tumors and *in vitro* cells, including sgRNA positive and sgRNA negative cells from unsorted populations, revealed numerous immune, stromal, and malignant cell populations across uniform manifold approximation and projection (UMAP) space (Fig. 1B; Supplementary Fig. 2, 3A-D). GL261 malignant cells from *in vivo* tumors were distinct from *in vitro* cultures, while GL261 cells from *in vivo* pre-infected or CED experiments clustered together in UMAP space (Fig. 1B,D, Supplementary Fig. 3A). We then identified cells expressing both sgRNAs from dual-guide vectors and found high recovery of sgRNAs in GL261 malignant cells across *in vivo* and *in vitro* experimental contexts (Fig. 1C-E). Analysis of sgRNA unique molecular identifier (UMI) counts confirmed single lentivirus vector integration events, as total sgRNA UMI counts were highly correlated with the sum of sgRNA UMI counts from sgRNA A and sgRNA B (Pearson R = 1.00) across each approach (Supplementary Fig. 3F). Mean cell coverage of individual sgRNA pairs ranged from 10.1 (CED no RT) to 86.3 (pre-infected no RT) cells per sgRNA pair (Supplementary Fig. 3E), yielding a total of 8257 (*in vitro*; duplicate cultures), 30878 (pre-infected; biological triplicates), and 2153 (CED; 5 pooled animals per condition) malignant GL261 cells for perturb-seq analysis.

Analysis of CRISPRi knockdown of target genes in GL261 cells revealed median on-target knockdown between 83% and 97% across experimental contexts (Fig. 1F). We then calculated per-sgRNA coverage across cells and found depletion of cells expressing sgRNAs with negative growth phenotypes and enrichment of cells expressing sgRNAs with positive growth phenotypes (Supplementary Fig. 3G), reflecting fitness effects that were also observed from traditional *in vitro* screens (Supplementary Fig. 1). Depletion and enrichment of cells was exacerbated for pre-infected *in vivo* perturb-seq experiments, which undermines sufficient capture of cells for transcriptional phenotyping of genes that are required for cell growth or survival (Supplementary Fig. 3G). By contrast, CED experiments allowed better recovery of essential genes such as *Myc* and *Mtor*, thus enabling transcriptional phenotyping of genes important in tumor maintenance (Supplementary Fig. 3G).

We then performed high dimensional phenotyping for each CRISPRi genetic perturbation using differential gene expression analysis (Methods). Differentially expressed genes were summarized using non-negative matrix factorization (NMF), revealing alteration of multiple gene expression modules across perturbations. Single-cell perturbations of essential genes (e.g. *Aurkb, Myc, Mtor*) decreased expression of cell cycle and growth gene modules across experimental contexts (Fig. 1G). Modules related to metabolism, cellular energetics, and cytokine signaling were dependent on whether perturbation occurred in CED compared to *in vitro,* or pre-infected contexts. Hypoxia related genes (e.g. *Pfkl, Eno3*) were suppressed following CED perturbations relative to *in vitro* or pre-infected perturbations ($p=4.93x10^{-12}$), while IL-2/Stat5 signaling was enriched following CED perturbation ($p=3.09x10^{-6}$) (Fig. 1G; Supplementary Fig. 4A). We then asked how each genetic perturbation modulated the transcriptional response to RT *in vitro* or *in vivo*. While RT uniformly skewed transcriptional states toward inflammation and growth arrest when combined with genetic perturbations *in vitro*, *in vivo* perturbation (pre-infected and CED) resulted in more heterogenous activation of these pathways (Fig. 1H). CED perturbation of radiation sensitizing hits (e.g. *Xrcc5, Shc1, Bard1*) attenuated DNA repair (p=0.00178) and p53 responses ($p=1.39x10^{-7}$), as well as TLR4 signaling ($p=5.60x10^{-12}$) and cholesterol homeostasis ($p=6.71x10^{-6}$) after RT, in contrast to *in vitro* and even pre-infected perturb-seq that primarily showed upregulation of these pathways in combination with RT (Supplementary Fig. 4B). These gene module expression changes were preserved after downsampling cells to normalize unequal cell sampling across experimental contexts (Methods; Supplementary Fig. 4C,D). Thus, *in vivo* genetic perturbation of GBM cells by

CED in a physiological context uniquely reveals the roles of radiation sensitizing and resistance genes *in vivo*, as well as rewiring of transcriptional responses following radiotherapy. These data demonstrate the utility of multiplexed *in vivo* perturbations paired with rich phenotyping for the study of disease and response to stimuli.

As cancers comprise both malignant and non-malignant host cells of the stroma or immune microenvironment, we asked whether CED perturb-seq could be applied toward stromal or immune microenvironment cells in GBM tumors. To that end, we used the SB28 syngeneic mouse GBM model, which is driven by *Nras* overexpression and establishes a myeloid cell-rich tumor immune microenvironment similar to human GBM[16,17]. SB28 cells that did not express CRISPRi machinery were transplanted intracranially into immunocompetent mice constitutively expressing dCas9-KRAB[18], enabling selective knockdown of genes in microenvironment cells but not in malignant cells (Fig. 2A). Target genes were selected for perturbation based on cell type-specific expression or function as master regulators of immune lineage (Supplementary Fig. 5). We delivered a lentiviral sgRNA library by CED into SB28 tumors, dissected tumors 5 days following CED, and performed scRNA-seq of unsorted tumors. Analysis revealed a diversity of non-cancer cell types (e.g. macrophages, astrocytes, endothelial cells) within the tumor microenvironment, existing alongside SB28 cells, which were readily distinguishable by *Nras* overexpression (Fig. 2B,D). Consistent with their high abundance in SB28 allografts, macrophages expressed the majority of sgRNAs in these tumors (Fig. 2C-D). We then analyzed CRISPRi knockdown of target genes in macrophages, which revealed repression of target genes normally expressed in this cell type (Fig. 2E; Supplementary Fig. 5). We specifically investigated the consequences of perturbing the phosphatase *Ptprc* in macrophages *in vivo* (Fig. 2F). *Ptprc* knockdown resulted in downregulation of genes associated with inflammation (Fig. 2F), consistent with its known role in innate immunity signaling[19]. To determine if genetic perturbation could influence cell-cell interactions within SB28 intracranial tumors, we identified putative cell-cell interactions using CellChat[20] (Methods) and overlapped candidate ligand-receptor pairs with differentially expressed genes in macrophages following *Ptprc* suppression. Following *Ptprc* knockdown, *Cxcl10* and *Cxcl9* decreased, leading to diminished interactions between macrophages and T cells ($p=0.0061$), as well as macrophages and endothelial cells ($p=0.0068$) (Fig. 2G). *Ptprc* knockdown in macrophages also abrogated cell-cell interactions through suppression of *Fn1, Edn1,* and *Ptprc* itself ($p=0.00011$), supporting the role of *Ptprc* as a regulator of paracrine interactions within tumors and demonstrating that non-cancer cell types present in the tumor microenvironment can be perturbed and then phenotyped using our *in vivo* perturb-seq approach.

In summary, we demonstrate that *in vivo* genetic perturbation combined with single cell phenotyping enables rich multiplexed analysis of phenotypes in cancer cells and immune cells. We uncover context-dependent transcriptional changes *in vivo* versus *in vitro*, as well as context-specific rewiring of transcriptional programs following radiotherapy. Direct perturbation of the tumor immune microenvironment also demonstrates the ability to alter and measure signaling pathways that are important for cellular crosstalk within the complex milieu of GBM tumors, which inform future studies of multicellular biology.

Figures

Figure 1: In vivo perturb-seq enables rich phenotyping of biologic drivers of glioblastoma

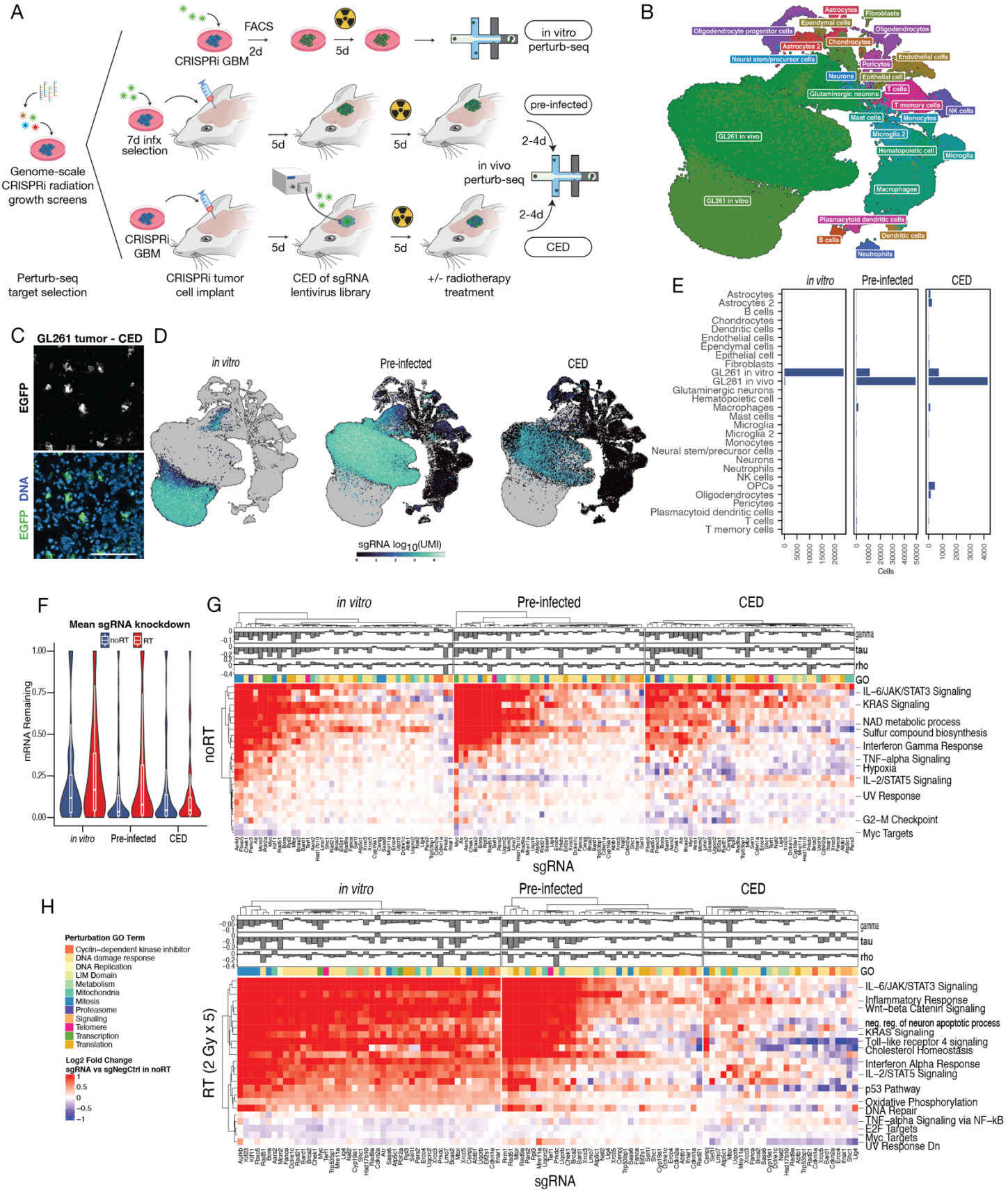

Figure 1. *In vivo* perturb-seq enables rich phenotyping of biologic drivers of GBM. A) Schematic of parallel *in vitro* and *in vivo* perturb-seq (either pre-infected or CED) in orthotopic GBM models against target genes nominated by genome-scale CRISPRi screens, followed by treatment with or without 2 Gy x 5 fractions

of radiotherapy. **B)** Integrated scRNA-seq UMAP of malignant and stromal/microenvironment cells from orthotopic GL261 tumors and GL261 cell cultures outlined in (A). **C)** Confocal image of GL261 orthotopic tumor transduced with a sgRNA library tagged with EGFP. Scale bar, 100 μm. **D)** Integrated scRNA-seq UMAP from (B) overlayed with sgRNA expression levels for *in vitro*, pre-infected, and CED perturb-seq. **E)** Number of sgRNA positive cells for each cell type across experimental contexts. **F)** Distribution of mean on-target knockdown levels for all perturbations across contexts and treatment conditions. Boxplots show 1st quartile, median, and 3rd quartile; whiskers represent 1.5 inter-quartile range. **G)** NMF heatmap of gene expression modules (rows) following sgRNA perturbations (columns) across experimental contexts without radiotherapy. Top bar charts show growth (gamma), radiation (tau), and radiation:growth ratio (rho) *in vitro* screen phenotypes. Gene ontology of perturbed target genes indicated. **H)** Heatmap of gene expression modules (rows) following sgRNA perturbations (columns) as in (G) across experimental contexts with radiotherapy. Expression changes are normalized to non-targeting control sgRNAs in the no RT condition.

Figure 2: In vivo perturb-seq of tumor immune microenvironment

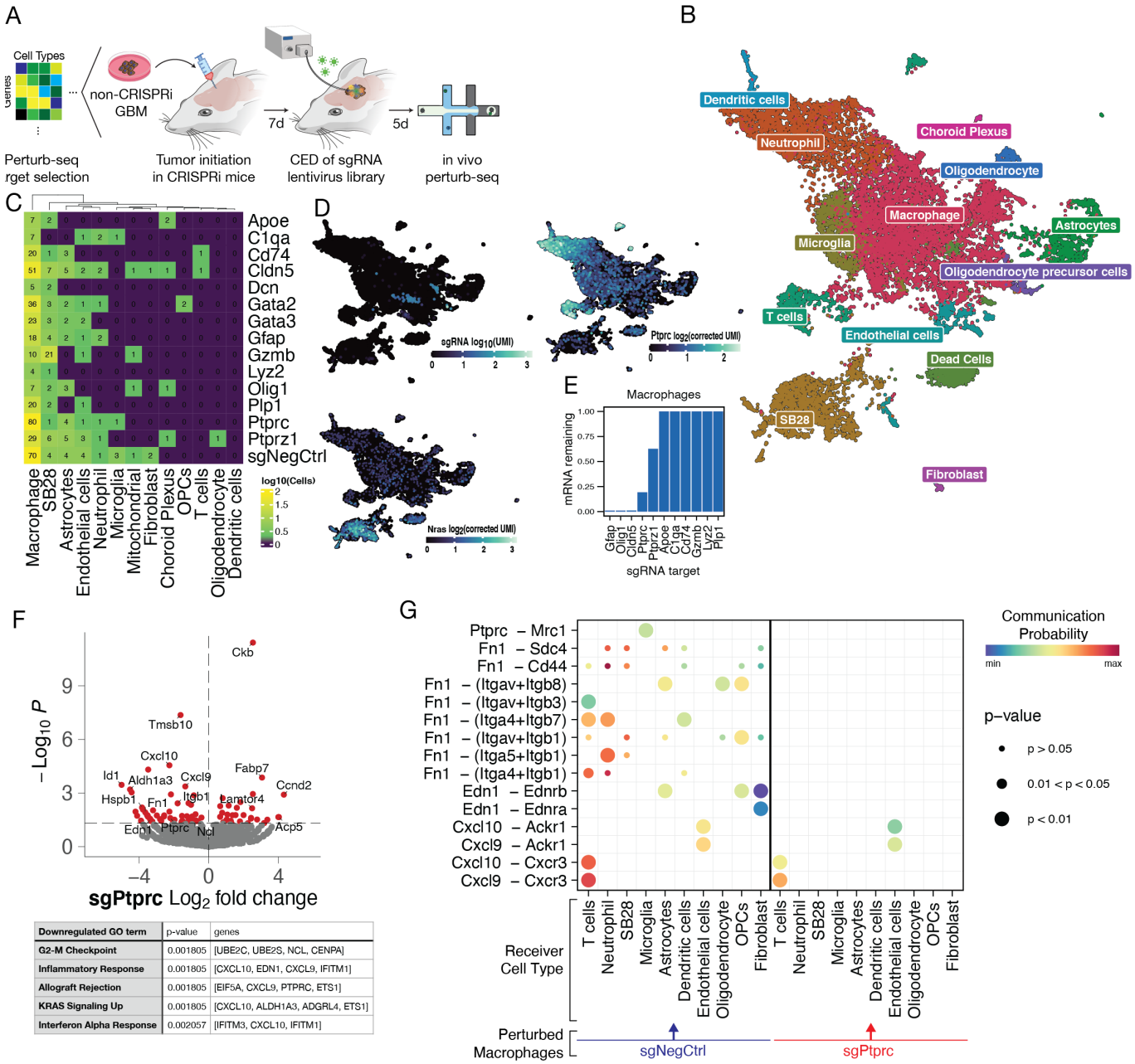

Downregulated GO term	p-value	genes
G2-M Checkpoint	0.001805	[UBE2C, UBE2S, NCL, CENPA]
Inflammatory Response	0.001805	[CXCL10, EDN1, CXCL9, IFITM1]
Allograft Rejection	0.001805	[EIF5A, CXCL9, PTPRC, ETS1]
KRAS Signaling Up	0.001805	[CXCL10, ALDH1A3, ADGRL4, ETS1]
Interferon Alpha Response	0.002057	[IFITM3, CXCL10, IFITM1]

Figure 2. *In vivo* perturb-seq of tumor immune microenvironment. A) Schematic of *in vivo* CED perturb-seq in orthotopic SB28 GBM models against 14 target genes nominated by scRNA-seq gene expression analysis. **B)** scRNA-seq UMAP of malignant and stromal/microenvironment cells from an orthotopic SB28 tumor. **C)** Number of sgRNA positive cells for each sgRNA perturbation across cell types identified in (B). **D)** UMAP featureplots of sgRNA, *Nras*, and *Ptprc* expression in SB28 tumors. **E)** On-target knockdown levels for perturbations of genes expressed in macrophages. **F)** Volcano plot of differential gene expression following *Ptprc* perturbation in macrophages along with significant gene ontology terms for downregulated genes. **G)** Ligand-receptor interactions inferred from transcriptional profiles of perturbed macrophages (either negative control or *Ptprc* sgRNA) along with target cells of the tumor microenvironment within the same SB28 tumor.

Supplementary Figure 1

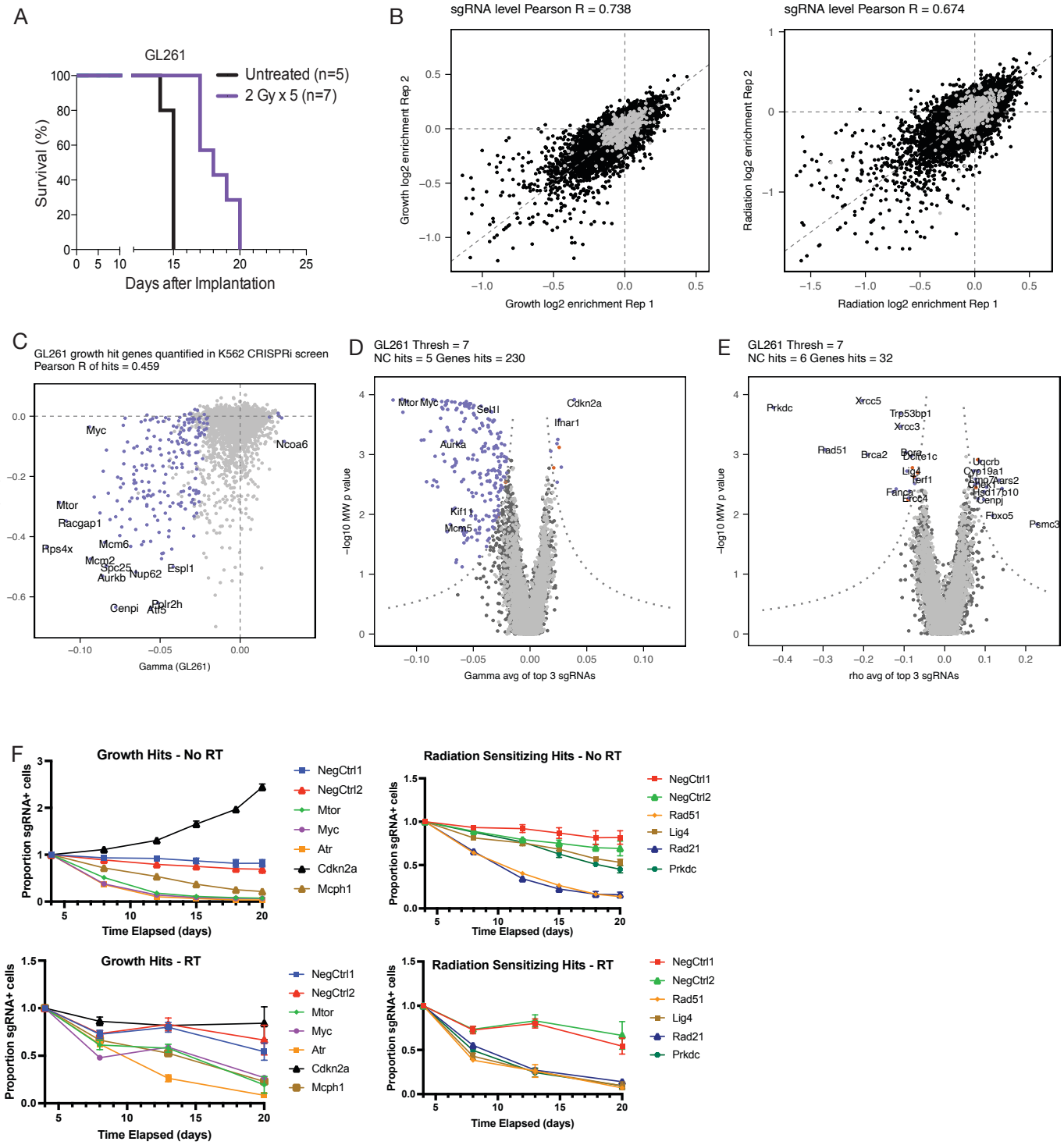

Supplementary Figure 1. CRISPRi screen and validation in GL261 GBM cells. A) Survival curves of GL261 intracranial tumor models treated with either fractionated radiotherapy (2 Gy x 5 fractions) to the whole brain or no treatment. **B)** Inter-replicate scatter plot of growth (left) and radiation (right) phenotypes for sgRNAs targeting genes (black) and non-targeting negative control sgRNAs (gray). **C)** Comparison of normalized growth phenotypes (gamma) in GL261 cells compared to published growth phenotypes in K562 cells from Horlbeck et al. 2016. **D)** Volcano plot of normalized growth (gamma) and **(E)** radiation:growth ratio (rho) phenotypes in GL261 cells. A discriminant threshold score of 7 was used for both screen analyses to nominate hit genes for *in vivo* perturb-seq. **F)** Internally controlled competitive growth assays validating growth (left) and radiation sensitizing (right) hit genes in the absence (top) or presence (bottom) of fractionated radiotherapy (2 Gy x 5 fractions) in GL261 cells expressing CRISPRi machinery.

Supplementary Figure 2

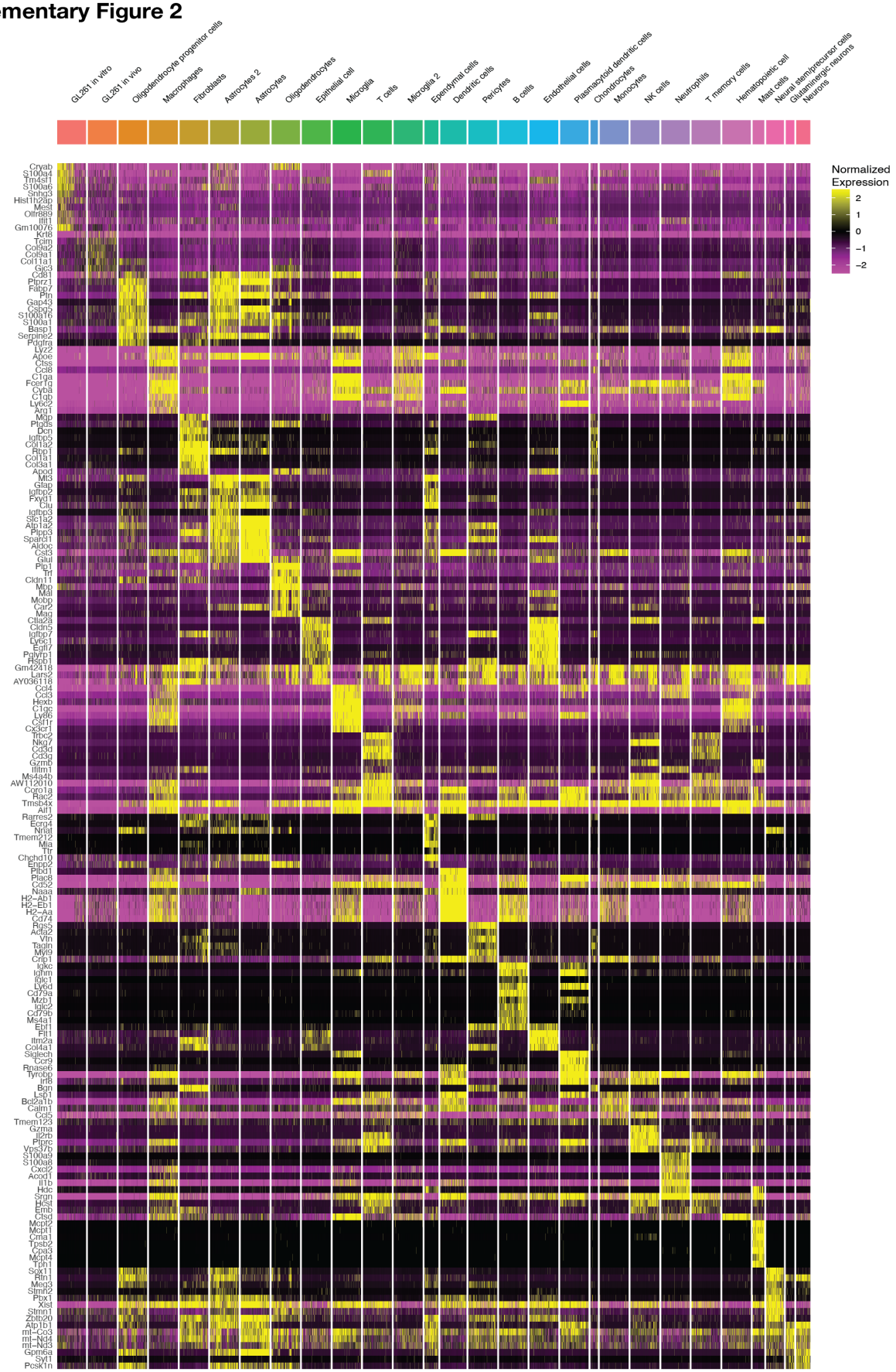

Supplementary Figure 2. Cell type marker gene expression in integrated GL261 tumors. Heatmap of marker gene expression for each cell type identified by scMRMA with manual annotation of GL261 *in vitro* and *in vivo* malignant cells. Expression values represent SCTransform residuals (normalized expression).

Supplementary Figure 3

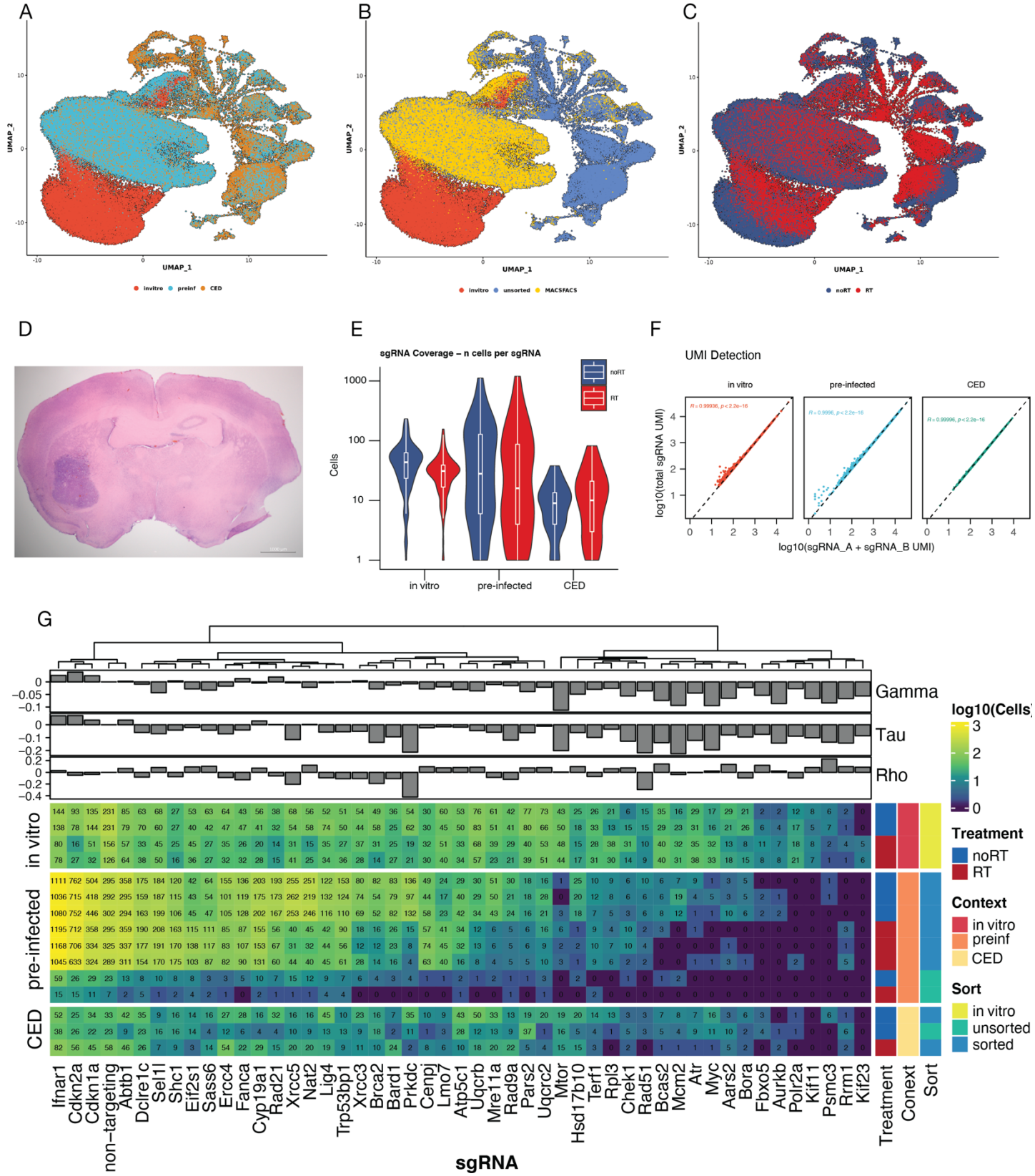

Supplementary Figure 3. Integrated analysis of *in vivo* perturb-seq in GL261 GBM cells. A) Integrated scRNA-seq UMAP of malignant and stromal/microenvironment cells from orthotopic GL261 tumors and GL261 cell cultures outlined in Fig. 1B, labeled according to their context (*in vitro*, pre-infected, CED), **(B)** whether cells were subjected to MACS negative selection followed by FACS for sgRNA transduction, **(C)** or treatment

condition (noRT = control; RT = 2 Gy x 5 fractions radiotherapy). **D)** Hematoxylin and eosin staining of GL261 orthotopic tumor centered in the right striatum. Scale bar, 1000 μm. **E)** Distribution of the number of cells expressing each sgRNA among GL261 malignant cells expressing CRISPRi machinery in either *in vitro,* pre-infected, or CED experimental context. **F)** Scatter plots comparing total sgRNA UMI's to the sum of UMI's corresponding to the expected sgRNA A and sgRNA B for each targeted gene, across experimental contexts. **G)** Heatmap of per-sgRNA coverage for each targeted gene in GL261 cells across contexts. Numbers represent number of cells expressing both sgRNAs against each target gene. Top bar charts show growth (gamma), radiation (tau), and radiation:growth ratio (rho) *in vitro* screen phenotypes. Each row of the heatmap shows an individual replicate experiment for either the *in vitro* (n = 2 biological replicate cultures per condition), pre-infected (n = 3 biological replicate tumors per condition), and CED (n = 5 replicate animals pooled per condition).

Supplementary Figure 4

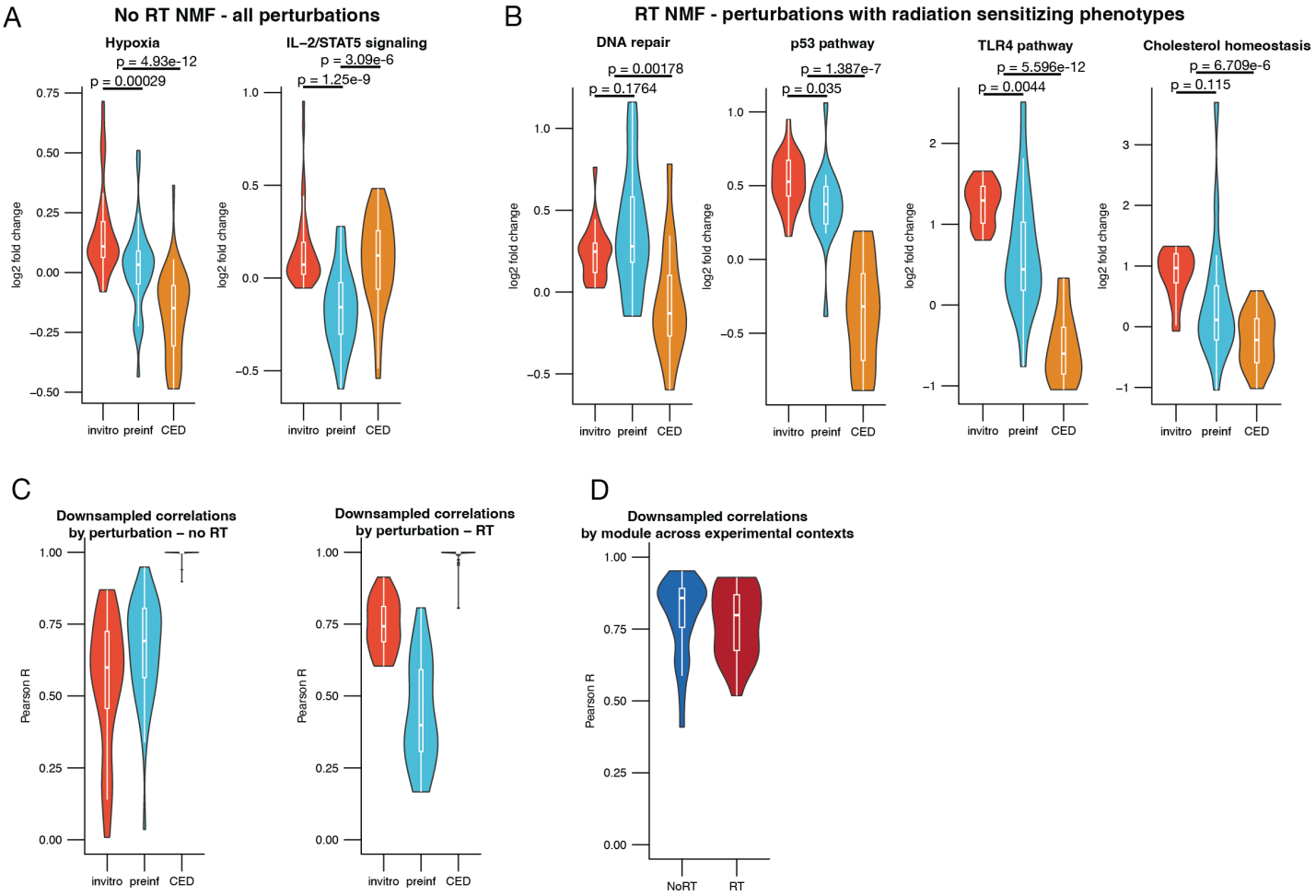

Supplementary Figure 4. Gene module expression changes following multiplex perturbations. A) Distribution of log2 fold changes for gene expression modules following NMF in the no RT condition, normalized to non-targeting control sgRNAs in the no RT condition. **B**) Distribution of log2 fold changes for gene expression modules following NMF in the RT condition, for radiation sensitizing hits (rho < 0) normalized to non-targeting control sgRNAs in the no RT condition. **C)** Distribution of Pearson correlation coefficients for perturbations across gene module expression changes, comparing all cells per perturbation to the set of downsampled cells per perturbation such that each perturbation is represented by equal numbers of cells across experimental contexts. **D**) Distribution of Pearson correlation coefficients for gene modules across perturbations, comparing all cells per gene module to the set of downsampled cells such that each perturbation is represented by equal numbers of cells across experimental contexts. Boxplots show 1st quartile, median, and 3rd quartile; whiskers represent 1.5 inter-quartile range. P values represent two-sided Student's *t* test.

Supplementary Figure 5

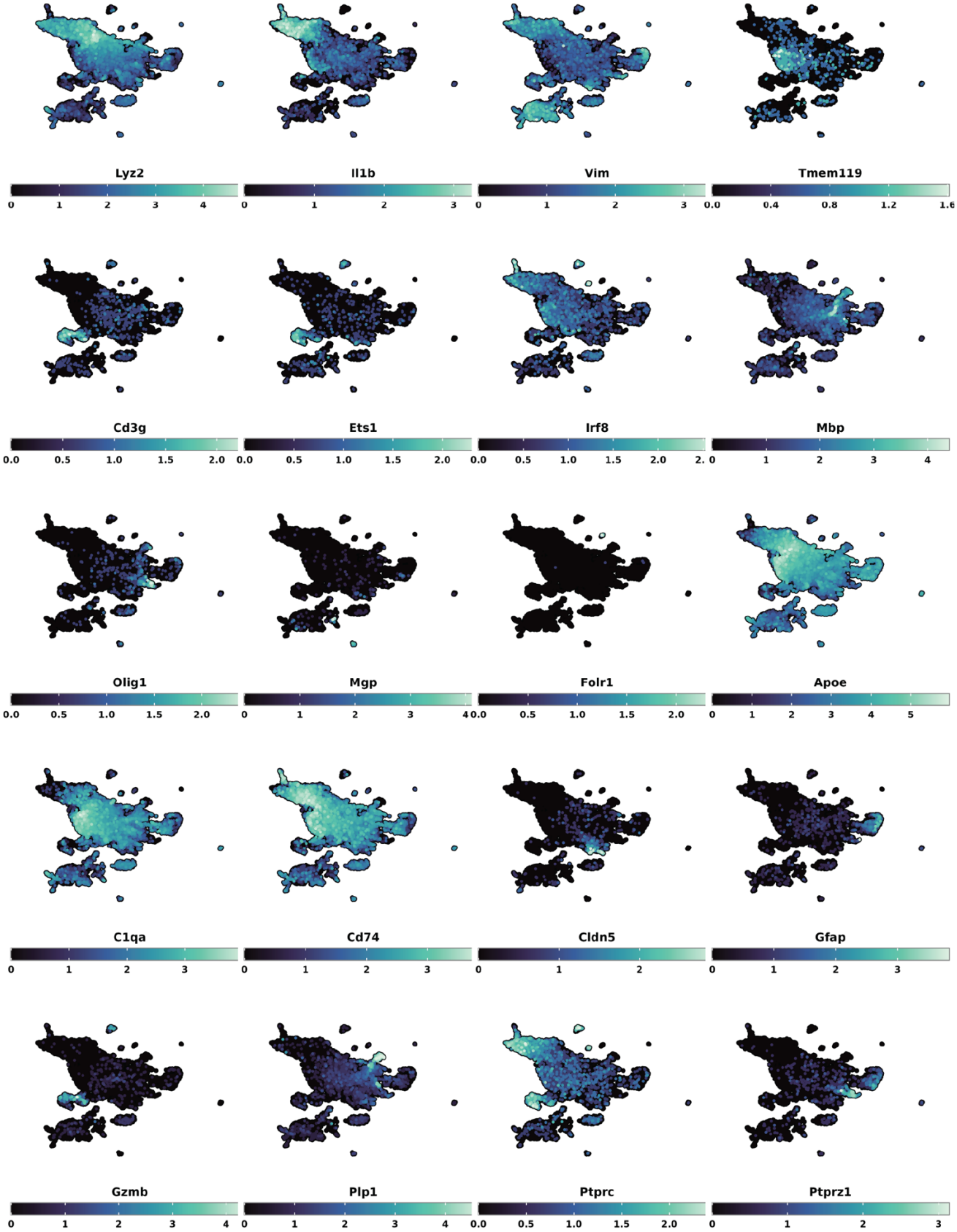

Supplementary Figure 5. Cell type marker gene expression in SB28 tumor microenvironment. Gene expression featureplots of marker genes or genes selected for sgRNA targeting in SB28 orthotopic tumor cells, overlayed on UMAP coordinates derived in Fig. 2B. Expression values represent log2 corrected UMI's.

Supplementary Table 1. *In vitro* growth and radiation phenotypes from pooled CRISPRi screens in GL261

Supplementary Table 2. *sgRNA libraries used for in vivo perturb-seq*

Data Availability
All sequencing data have been deposited on NCBI SRA accession number PRJNA1005229.

Code Availability
Computational code has been deposited on Github at https://github.com/GilbertLabUCSF/gbm_perturb.

Acknowledgements
SJL was funded by the Conquer Cancer – The Sontag Foundation Young Investigator Award. Sequencing was performed at the UCSF CAT, supported by UCSF PBBR, RRP IMIA, and NIH 1S10OD028511-01 grants. SJL, WAW, DRR and LAG acknowledge support from UCSF's Marcus Program in Precision Medicine Innovation. WAW acknowledges support from the Samuel Waxman Cancer Research Foundation, and Cancer Research UK Brain Tumour Award A28592.

Author Contributions
All authors contributed substantially to the inception, design, implementation, analysis, or writing of this report. All authors approved the manuscript. SJL, LG, DRR, WW, and TO designed the study and analyses. Experiments were performed by SJL, JP, TCC, KS, TO'L, TO, DRR, and LG. Computational data analyses were performed by SJL, CZ, AB, and DW. The study was supervised by SJL, DL, TO, MSB, WW, DRR, and LG. The manuscript was prepared by SJL, LG, and CZ with input from all authors.

Competing interests statement
The authors declare no competing interests.

References

1. Przybyla, L. & Gilbert, L. A. A new era in functional genomics screens. *Nat. Rev. Genet.* **23**, 89–103 (2022).

2. Lara-Astiaso, D. *et al.* In vivo screening characterizes chromatin factor functions during normal and malignant hematopoiesis. *Nat. Genet.* 1–13 (2023) doi:10.1038/s41588-023-01471-2.

3. Dhainaut, M. *et al.* Spatial CRISPR genomics identifies regulators of the tumor microenvironment. *Cell* (2022) doi:10.1016/j.cell.2022.02.015.

4. Adamson, B. *et al.* A Multiplexed Single-Cell CRISPR Screening Platform Enables Systematic Dissection of the Unfolded Protein Response. *Cell* **167**, 1867-1882.e21 (2016).

5. Replogle, J. M. *et al.* Combinatorial single-cell CRISPR screens by direct guide RNA capture and targeted sequencing. *Nature Biotechnology* **38**, 954–961 (2020).

6. Replogle, J. M. *et al.* Mapping information-rich genotype-phenotype landscapes with genome-scale Perturb-seq. *Cell* **185**, 2559-2575.e28 (2022).

7. Datlinger, P. *et al.* Pooled CRISPR screening with single-cell transcriptome readout. *Nature Methods* **14**, 297–301 (2017).

295 8. Dixit, A. *et al.* Perturb-Seq: Dissecting Molecular Circuits with Scalable Single-Cell RNA Profiling of Pooled
296 Genetic Screens. *Cell* **167**, 1853-1866.e17 (2016).

297 9. Liu, S. J. *et al.* Epigenetic reprogramming shapes the cellular landscape of schwannoma. *bioRxiv*
298 2022.12.23.521842 (2022) doi:10.1101/2022.12.23.521842.

299 10. Low, J. T. *et al.* Primary brain and other central nervous system tumors in the United States (2014-2018):
300 A summary of the CBTRUS statistical report for clinicians. *Neuro-oncology Pract* **9**, 165–182 (2022).

301 11. Neftel, C. *et al.* An Integrative Model of Cellular States, Plasticity, and Genetics for Glioblastoma. *Cell* 1–
302 37 (2019) doi:10.1016/j.cell.2019.06.024.

303 12. Jin, X. *et al.* In vivo Perturb-Seq reveals neuronal and glial abnormalities associated with autism risk
304 genes. *Science* **370**, eaaz6063 (2020).

305 13. Jahangiri, A. *et al.* Convection-enhanced delivery in glioblastoma: a review of preclinical and clinical
306 studies. *J Neurosurg* **126**, 191–200 (2017).

307 14. Bankiewicz, K. S. *et al.* Convection-Enhanced Delivery of AAV Vector in Parkinsonian Monkeys; In Vivo
308 Detection of Gene Expression and Restoration of Dopaminergic Function Using Pro-drug Approach. *Exp.*
309 *Neurol.* **164**, 2–14 (2000).

310 15. Replogle, J. M. *et al.* Maximizing CRISPRi efficacy and accessibility with dual-sgRNA libraries and
311 optimal effectors. *eLife* **11**, e81856 (2022).

312 16. Simonds, E. F. *et al.* Deep immune profiling reveals targetable mechanisms of immune evasion in
313 immune checkpoint inhibitor-refractory glioblastoma. *J Immunother Cancer* **9**, e002181 (2021).

314 17. Kosaka, A., Ohkuri, T. & Okada, H. Combination of an agonistic anti-CD40 monoclonal antibody and the
315 COX-2 inhibitor celecoxib induces anti-glioma effects by promotion of type-1 immunity in myeloid cells and T-
316 cells. *Cancer Immunol Immunother* **63**, 847–857 (2014).

317 18. Lindtner, S. *et al.* Genomic Resolution of DLX-Orchestrated Transcriptional Circuits Driving Development
318 of Forebrain GABAergic Neurons. *Cell Rep.* **28**, 2048-2063.e8 (2019).

319 19. Barashdi, M. A. A., Ali, A., McMullin, M. F. & Mills, K. Protein tyrosine phosphatase receptor type C
320 (PTPRC or CD45). *J. Clin. Pathol.* **74**, 548–552 (2021).

321 20. Jin, S. *et al.* Inference and analysis of cell-cell communication using CellChat. *Nat Commun* **12**, 1088
322 (2021).

323
324
325
326
327
328
329
330
331
332
333
334
335

Online Methods

In vitro CRISPRi screens, analysis, and validation

HEK-293T cells were cultured in Dulbecco's Modified Eagle Medium (Gibco, #11960069) supplemented with 10% fetal bovine serum (FBS) (Life Technologies, #16141). Cell cultures were authenticated by STR analysis at the UC Berkeley DNA Sequencing Facility, as well as routinely tested for mycoplasma using the MycoAlert Detection Kit (Lonza, #75866-212). GL261 cells were cultured in Dulbecco's Modified Eagle Medium (Gibco, #11960069) supplemented with 10% fetal bovine serum (FBS) (Life Technologies, #16141), and GL261 cells stably expressing the CRISPR interference (CRISPRi) machinery dCas9-KRAB were generated as previously described[1,2]. Lentivirus was produced from transfected HEK293T cells with packaging vectors (pMD2.G #12259, Addgene, and pCMV-dR8.91, Trono Lab) following the manufacturers protocol (#MIR6605, Mirus). GL261 GBM cells were transduced with lentivirus harboring SFFV-dCas9-BFP-KRAB, and the top ~25% of cells expressing BFP were FACS sorted, expanded, and FACS sorted a second time.

For genome-scale CRISPRi screening *in vitro*, we used a mouse sgRNA library[3] comprising 27,300 sgRNAs targeting 5,234 cancer related and/or druggable genes, in addition to 530 non-targeting control sgRNAs. Pooled lentivirus was generated as above, and GL261 cells were transduced using spin-infection of viral supernatant of a MOI of ~0.1 at 1000g for 120 minutes. 4 days of puromycin selection (1.5 µg/mL) was performed, followed by 2 days of growth in non-puromycin 10% FBS in DMEM media. Two replicates of each screen were performed at a coverage of 525x cells per sgRNA, in both no radiation and radiation (2 Gy x 5 fractions delivered every other day) treatment conditions. Infection efficiency was evaluated by measuring GFP positivity on flow cytometry. Initial (T0) cell populations were then frozen in 10% DMSO and processed for genomic DNA using the NucleoSpin Blood XL Kit (Machery-Nagel, #740950.50). Endpoint cell pellets were harvested for genomic DNA after 12 days of growth, corresponding to ~7 and ~5 doublings in the no radiation and radiation conditions, respectively. sgRNA sequencing libraries were prepared using NEBNext Ultra II Q5 PCR MasterMix (New England Biolabs, #M0544L) and sequenced on an Illumina NextSeq-500 as previously described[59].

sgRNAs with fewer than 100 reads at T0 were removed from subsequent analysis. Enrichment or depletion of sgRNA abundances were determined by down sampling trimmed sequencing reads to equivalent amounts across all samples. Growth phenotype (gamma) was defined as log2(sgRNA count T12 (0Gy) / sgRNA count T0) minus median sgNTC log2(sgRNA count T12 (0Gy) / sgRNA count T0), then normalized by the number of cell doublings, as previously described[1]. Radiation phenotype (tau) was defined as log2(sgRNA count T12 (2Gy x 5) / sgRNA count T0) minus median sgNTC log2(sgRNA count T12 (2Gy x 5) / sgRNA count T0), then normalized by the number of cell doublings in the radiation screen. Radiation:growth ratio phenotype (rho) was defined as log2(sgRNA count T12 (2Gy x 5) / sgRNA count T12 (0 Gy)). Gene-level phenotypes were summarized at the mean of the top 3 sgRNAs against a given gene, ranked according to screen phenotype. Statistical significance was calculated using the Mann-Whitney-U test for a given perturbation compared to the sgRNA distribution of the non-targeting control sgRNAs (Supplementary Table 1). A discriminant threshold of 7, derived from the product of normalized gene phenotype and -log10(p-value), corresponding to an empiric false discovery rate of ~2%, was selected for hit definitions[1]. To ascertain the fidelity of our mouse cell CRISPRi screens, we overlapped gamma phenotypes (without radiotherapy treatment) in our GL261 screens with gamma phenotypes from K562 CRISPRi cells subjected to genome-wide human CRISPRi growth screens[1].

Internally controlled competitive growth assays were then performed to validate CRISPRi screen hits. GL261 cultures were partially transduced with sgRNA expression lentiviruses with a GFP tag (Addgene 187241)[4], and the percentage of sgRNA positive cells were measured over time using flow cytometry, in the presence or absence of radiotherapy (2 Gy x 5 fractions).

Intracerebral tumor establishment

Five to six-week-old female C57/B6 (Envigo Laboratories, Livermore, CA), housed under aseptic conditions, received intracranial tumor cell injection as previously described[5], and as approved by the University of California San Francisco Institutional Animal Care and Use Committee. For the microenvironment perturb-seq, mice expressing dCas9-KRAB from the H11 locus with a mCherry tag (JAX # 030000) were utilized. Briefly, mice were anesthetized by combination of intraperitoneal injection of a mixture containing ketamine (100 mg/kg) and xylazine (10 mg/kg), and inhalation of isoflurane. The scalp was surgically prepped, and a skin incision ~10 mm in length was made over the middle frontal to parietal bone. The surface of the skull was exposed so that a small hole was made 3.0mm to the right of the bregma and just in front of the coronal suture

with a 25-gauge needle. A 26-gauge needle attached to a Hamilton syringe was inserted into the hole in the skull. The needle was covered with a sleeve that limits the injection depth to 3-4mm. 3 μL of tumor cell suspension (300,000 GL261 cells; 30,000 SB28 cells) was injected into the right caudate putamen at a rate of 1 μL/min by free hand. The skull surface was then swabbed with hydrogen peroxide before the hole was sealed with bone wax to prevent reflux. The scalp was closed with surgical staples.

Bioluminescence imaging of intracranial tumor growth

For bioluminescence imaging (BLI), mice were anesthetized with inhalation of isoflurane, then administered 150 mg/kg of luciferin (D-luciferin potassium salt, Gold Biotechnology, St. Louis, MO) via intraperitoneal injection. Ten minutes after luciferin injection, mice were examined for tumor bioluminescence with an IVIS Lumina imaging station and Living Image software (Caliper Life Sciences, Alameda, CA), and intracranial regions of interest were recorded as photons per second per steradian per square cm[5].

Convection enhanced delivery of lentivirus

Convection enhanced delivery was performed as previously described[6]. Briefly, infusion cannulas were constructed with silica tubing (Polymicro Technologies, Phoenix, AZ) fused to a 0.1 ml syringe (Plastic One, Roanoke, VA) with a 0.5-mm stepped tip needle that protruded from the silica guide base. The syringe was loaded with 15 μL concentrated lentivirus produced using the LV-MAX Lentiviral Production System (Thermo Fisher #A35684) according to manufacturer's protocol, followed by 200x concentration using ultracentrifuge (Beckman L8-80M) at 25,000g for 2.5 hours at 4°C. The syringe was attached to a microinfusion pump (Bioanalytical Systems, Lafayette, Ind.), and the syringe with silica cannula was lowered through a puncture hole made in the skull[5,7], targeting the same region in the caudate putamen where tumor cells had been previously injected. The concentrated lentivirus was infused at a rate of 1 μL/min until a volume of 15 μL had been delivered. Cannulas were removed 2 minutes after completion of infusion.

Whole brain animal irradiation

Mice were anesthetized by combination of intraperitoneal injection of a mixture containing ketamine (100 mg/kg) and xylazine (10 mg/kg), and inhalation of 2.5% isoflurane with 1 liter of oxygen per minute for 5 minutes prior to being positioned on an irradiation platform located 16.3cm from a Cesium-137 source (J. L. Shepherd & Associates, San Fernando, CA). Animal subjects' eyes, respiratory tracts, and bodies were protected with lead shielding. Whole brain irradiation (2 Gy for 5 daily fractions) was delivered at a dose rate of 247 cGy/min[8]. After irradiation, animals were monitored until recovery from anesthesia. Following no radiation or radiation treatment, animals were sacrificed and brains were quickly removed from the skull, and the tumor mass was microdissected as previously described[5].

Imaging

Fluorescence microscopy was performed on a Zeiss LSM 800 confocal laser scanning microscope with Airyscan. Images were processed and quantified from at least 2 regions per condition using ImageJ9. Hematoxylin and eosin stained slides were imaged on a Zeiss Axio Zoom V16 light microscope.

In vitro and in vivo perturb-seq in malignant cells

Perturb-seq sgRNA libraries were designed by nominating 48 genes with radiation sensitizing, radiation resistance, negative growth, or positive growth phenotypes in *in vitro* CRISPRi screens as described above. Protospacer sequences were selected from the optimized mouse CRISPRi v2 library[3], and the top two scoring sgRNAs for each target gene based on depletion or enrichment phenotypes were cloned into dual sgRNA lentivirus expression vectors with direct capture tags (Addgene 187241)[4] using NEBuilder HiFi DNA Assembly Master Mix (New England Biolabs #E2621L) (Supplementary Table 2). Concentrated lentivirus of pooled sgRNA libraries were produced as described above.

For *in vitro* perturb-seq, GL261 cells expressing dCas9-KRAB were transduced with lentivirus at an MOI of ~0.1, and cells were FACS sorted (BD FACSAria Fusion) for GFP positivity 48 hours following transduction. Cell cultures were irradiated using a Cesium-137 source to 2 Gy x 5 fractions delivered daily, starting on same day of FACS. 12 hours following the final fraction of radiotherapy, cells were trypsinized and harvested in single cell suspension on the 10x Chromium Controller (10x Genomics, #1000204). Single-cell perturb-seq libraries were processed using the Chromium Next GEM Single Cell 3' GEM, Library & Gel Bead Kit v3.1 with Feature Barcoding (10x Genomics, #1000269), allowing direct capture of modified sgRNAs, and

446 sequenced on a illumina NovaSeq-6000. *In vitro* perturb-seq experiments were performed in biological
447 duplicate cultures for each treatment condition.
448 For pre-infected *in vivo* perturb-seq, GL261 cells expressing dCas9-KRAB were transduced with
449 lentivirus at an MOI of ~0.1 and were subjected to puromycin selection (1.5 µg/uL) for 3 days, starting 2 days
450 after transduction, followed by 2 days of growth in non-puromycin recovery media. 300,000 cells were
451 intracranially injected into each mouse as described above. Tumors were allowed to establish and expand for
452 5 days, and radiation (or no treatment) was delivered to a dose of 2 Gy x 5 daily fractions as described above.
453 For tumors of the no radiation arm, tumor harvest was performed 12 days following intracranial injection of
454 cells. For tumors of the radiation arm, tumor harvest was performed 2 days following completion of radiation
455 treatment, or 14 days total after intracranial injection of cells. Harvested tumors were minced and dissociated
456 to single cell suspension using the Papain Dissociation System (Worthington #LK003150) following
457 manufacturer's protocol without the use of ovomucoid protease inhibitor. Cell suspensions were passed through
458 a 70 µm strainer (Corning, #352350), centrifuged at 300g for 5 minutes, and resuspended in cold phosphate
459 buffered saline. To capture cells of the tumor microenvironment as well as sgRNA transduced malignant cells
460 *in vivo*, we processed a fraction of the dissociated tumor for immune cell depletion using CD11b MicroBeads
461 (Miltenyi Biotec #130-097-142) following manufacturer's protocol on LS Columns, followed by FACS sorting for
462 sgRNA positive cells tagged with GFP. Sorted cells as well as a separate fraction of the dissociated tumor that
463 was not CD11b depleted or FACS sorted were processed for scRNA-seq with direct capture of sgRNA tags
464 using 10x Chromium Controller (10x Genomics, #1000204). Single cell perturb-seq libraries were processed
465 as described for *in vitro* perturb-seq. Pre-infected *in vivo* perturb-seq experiments were performed in biological
466 triplicate tumors.
467 For CED *in vivo* perturb-seq, GL261 cells expressing dCas9-KRAB were intracranially injected into mice
468 as described above. Tumors were allowed to establish and expand for 5 days, and CED of concentrated
469 lentivirus was performed as described above. For the radiation treatment arm, whole brain irradiation was
470 delivered to a dose of 2 Gy x 5 daily fractions as described above, initiating 2 days following CED to allow
471 lentiviral transduction and sgRNA expression. For tumors of the no radiation arm, tumor harvest was performed
472 5 days following CED, for a total of 12 days following implantation of cells. For tumors of the radiation arm,
473 tumor harvest was performed 2 days following completion of radiation treatment, or 14 days total after
474 intracranial injection of cells. Harvested tumors were minced and dissociated to single cell suspension as
475 described for pre-infected *in vivo* perturb-seq. 5 tumors from biological replicate animals in each treatment arm
476 were pooled to increase sgRNA positive cell recovery (0.7-1.1% sgRNA positive per pool by FACS). From these
477 pools of dissociated cells, separate immune cell depletion followed by FACS sorting for GFP and unenriched
478 populations were captured for scRNA-seq with direct capture of sgRNAs as described above. Single cell
479 perturb-seq libraries were processed as described for *in vitro* perturb-seq.
480
481 *In vivo perturb-seq in tumor microenvironment cells*
482 Microenvironment perturb-seq sgRNA libraries were designed by nominating 14 genes that were either
483 overexpressed in various cell types from scRNA-seq of SB28 orthotopic tumors, or by their known gene function
484 as key transcription factors in lineage development. Protospacer sequences were selected from the optimized
485 mouse CRISPRi v2 library[3] by their predicted rank order, and the top 2-3 sgRNAs were individually cloned into
486 single sgRNA expression vectors with direct capture cs1 sequences (Addgene # 122238)[9] using restriction
487 digest (BstXI and BlpI) and T4 ligation (NEB # M0202M). Concentrated lentivirus of pooled sgRNA was
488 produced as described above. SB28 cells[10] without CRISPRi machinery were intracranially injected into the
489 H11-dCas9-KRAB mice (JAX # 030000) as described above, and CED of concentrated lentivirus was
490 performed as described above 7 days after tumor implantation. 5 days following CED, tumors were harvested,
491 minced, and dissociated to single cell suspension using the Papain Dissociation System (Worthington
492 #LK003150) following manufacturer's protocol without the use of ovomucoid protease inhibitor. Cell
493 suspensions were passed through a 70 µm strainer (Corning, #352350), centrifuged at 300g for 5 minutes, and
494 resuspended in cold phosphate buffered saline. To capture the full spectrum of cell types including sgRNA
495 positive and negative cells, single cell suspensions were processed directly for scRNA-seq with direct capture
496 of sgRNA tags using 10x Chromium Controller (10x Genomics, #1000204). Single-cell perturb-seq libraries
497 were processed using the Chromium Next GEM Single Cell 3' GEM, Library & Gel Bead Kit v3.1 with Feature
498 Barcoding (10x Genomics, #1000269), allowing direct capture of modified sgRNAs, and sequenced on a
499 illumina NovaSeq-6000. Tumor microenvironment perturb-seq was performed in biological duplicate animals.
500

501
502 ***Perturb-seq computational analysis***
503
504 *Pre-processing, sgRNA calling, cell type identification*
505 Library demultiplexing, gene expression read alignment to human genome GRCh38, UMI quantification,
506 and sgRNA assignment and quantification were performed in Cell Ranger version 6.1.2 with sgRNA barcoding
507 (10X Genomics). Single cell RNA-seq analysis was performed in Seurat version 4.3.0[11] in R version 4.3.1. For
508 analysis of cellular heterogeneity across all perturb-seq experiments, including malignant cells and
509 microenvironment, cells with greater than 200 detected features were retained. RNA expression data was
510 transformed using SCTransform[12] in Seurat, and expression featureplots show log2 UMI's corrected by
511 SCTransform. Expression heatmaps of scRNA-seq data show SCTransform residuals (normalized expression).
512 Uniform manifold approximation and projection (UMAP) was performed using the Seurat function RunUMAP
513 using the first 30 dimensions from principal component analysis of the transformed expression data, using
514 parameters (min.dist = 0.7). Cell type identification of stromal and microenvironment cells was performed using
515 single cell multiresolution marker-based annotation (scMRMA) version 1.0[13], using the PanglaoDB mouse cell
516 types reference[14], with manual confirmation of known marker gene specificity. To deconvolve malignant tumor
517 cells from stromal tissue with potentially similar RNA expression profiles, we integrated scRNA-seq data from
518 our *in vitro* cultures and *in vivo* experiments to allow manual annotation of *in vitro* GBM cells, as these were
519 processed in separate 10x lanes and therefore could be distinguished by metadata. Similarly, sgRNA positive
520 cells from the pre-infected perturb-seq experiments could be readily identified as malignant GBM cells, as these
521 were transduced with sgRNA prior to *in vivo* implantation. Using these pre-defined cell clusters of malignant
522 cells, projection of cells from the CED perturb-seq experiment onto an integrated UMAP space demonstrated
523 a highly abundant population of cells which co-clustered with malignant cells from the pre-infected perturb-seq
524 experiment, and therefore these cells well identified as *in vivo* malignant GBM cells.
525 Cells were retained for further analysis if they expressed both the expected sgRNA A and sgRNA B
526 against a given target gene, corresponding to the sgRNAs of the dual sgRNA expression vector. Target gene
527 knockdown was quantified by library normalizing the untransformed transcriptome UMIs of each sgRNA
528 positice cell and obtaining the mean expression of each gene across all cells belonging to a given sgRNA within
529 each individual GEM group. RNA remaining for each gene target was calculated by dividing the pseudobulk
530 expression in on-target cells with cells expressing non-targeting negative control sgRNAs, with a pseudocount
531 of 0.1 added to each component. RNA remaining values were capped at a ceiling of 1.0. Expression
532 featureplots were generated using SCPubr version 1.1.2[15].
533
534 *Differential gene expression analysis*
535 First, we filtered the expression objects as follows: For each differential expression run, we isolated
536 cells by the desired experimental context (*in vitro,* pre-infected, CED), selected for FACS sorted only cells in
537 the pre-infected context, and selected cells with sgRNA expression called for both expected sgRNAs against a
538 given target gene. We removed cells with perturbations that had coverage of less than or equal to 5 cells. Next,
539 we used the default findDE method from the DElegate package version 1.1.0[16] to find differentially expressed
540 genes. DElegate is a wrapper around DESeq2 that adapts bulk sequencing methods for single cell data. The
541 effect of running findDE is to run DESeq2 with the Wald test on randomly assigned 3-group pseudoreplicates.
542 findDE's input is a Seurat object and metadata specifications for a group of interest and a control group to
543 measure against. We ran findDE with two different control group schemes: in one, which in the rest of this
544 methods section we call "noRTNormalized," we compared cells with a particular perturbation + radiation and
545 cells with that perturbation + no radiation to the non-targeting perturbation + no radiation. In the other, which
546 we'll call "condNormalized," we compared cells with perturbation + radiation to non-targeting + radiation and
547 cells with perturbation + no radiation to non-targeting + no radiation. Per perturbation, findDE's output is a CSV
548 file that provides—for each gene expressed in the cells compared—the following information: the gene name,
549 the average expression of the gene (using deseq:baseMean), the log2 fold change, the test statistic, the p-
550 value, the FDR adjusted p-value, among other columns. We provide full ouput CSVs in the data/deseq directory
551 on GitHub (repository https://github.com/GilbertLabUCSF/gbm_perturb). We repeated this DElegate::findDE
552 workflow for all perturbations across the three experimental contexts—*in vitro,* pre-infected, and convection
553 enhanced delivery—and the two normalization schemes—condNormalized and noRTNormalized—for six sets
554 of CSV files. Each set represented one experimental context paired with a normalization scheme. Each CSV
555 represented a comparison of expression between perturbed cells and the control cells. Heatmaps in Figure 1

556 are derived from noRTNormalized analysis. Next, we screened each of the resulting CSV sets to find the
557 differentially expressed genes. Within each set, we considered any gene that had an absolute value log2 fold
558 change of greater than 0.1 and an adjusted p-value of less than 0.05 to be differentially expressed. We took
559 the union of differentially expressed genes across relevant perturbations to form gene sets. In particular, for the
560 comparison of effects under no radiation and different contexts (Figure 1G), we took the union of all differentially
561 expressed genes from no radiation cells across the three contexts under the noRTNormalized scheme. For the
562 comparison of radiation-dependent reprogramming (Figure 1H), we took the union of all differentially expressed
563 genes from irradiated cells across all three contexts under the noRTNormalized scheme. Once a gene set was
564 identified, we used the data in the CSV outputs to generate a log2 fold change matrix where each column was
565 a perturbation/context combination and each row was a gene in the set. Cells in the matrix showed the DESeq
566 log2 fold change for that gene in cells with that perturbation and context. This matrix was the output taken into
567 non-negative matrix factorization.
568
569 *Non-negative matrix factorization*
570 We used non-negative matrix factorization (NMF) to extract gene modules from each gene set. To
571 prepare the data, we used Seurat's LogNormalize function to normalize the count data from the Seurat
572 expression objects, subsetting on context or treatment condition where necessary. Then, we filtered the
573 expression matrix to include only the genes in the input gene set and only perturbations that had DESeq
574 outputs: in other words, perturbations that passed our coverage filters. Next, we extracted the expression matrix
575 and collapsed it along the cell axis by averaging cells by their perturbation and context. For example, we
576 replaced all columns originating from cells that had an sgAars2 perturbation in the CED context to a single
577 column with the average of all such cells. Using R's base NMF package version 0.26, we ran NMF on the
578 expression matrix for rank k ranging from 2 to 40, with 60 NMF programs per k. The shown k was chosen based
579 on minimizing the mean squared error, reasonable stability as measured by a high cophenetic correlation
580 coefficient, and a biologically interpretable number of gene modules. Where choices abounded and there were
581 sufficient gene modules, we chose smaller k values to avoid overfitting. After obtaining the factorization with
582 optimal rank, we worked off the basis matrix W, within which each column corresponds to a gene module, each
583 row a gene, and the entries contributions for that gene to that gene module. We eliminated any genes that were
584 significantly zero-inflated in the basis matrix (those with mean expression across all clusters less than 0.01)
585 and genes with unidentified gene functions (those ending in -Rik or starting with Gm-). We grouped the
586 remaining genes into disjoint modules based on which NMF cluster they had the highest contribution in. To
587 annotate the gene modules, we submitted the genes in each to the EnrichR API version 3.2[17,18]. Each module
588 was labeled with the top term from the MSigDB Hallmark 2020 Gene Sets as well as GO Biological Process
589 2021 gene sets. Lastly, we collapsed the genes from the log2 fold change matrix generated from differential
590 expression analysis by averaging log2 fold change within each gene module. These matrices are the basis for
591 Figures 1G and 1H.
592
593 *Downsampled Analysis*
594 To account for differences in cell sampling between *in vitro,* pre-infected, and CED perturbations, we
595 prepared downsampled differential expression output by modifying the preprocessing steps prior to running
596 DElegate's findDE. First, we removed perturbations with less than or equal to 5 cells. Then, we removed
597 perturbations that did not have coverage across all 3 experimental contexts. Finally, we found the experimental
598 context with the lowest coverage for each perturbation and randomly downsampled the number of cells in the
599 other two contexts to that number of cells.
600 We took the resulting Seurat object into the differential gene analysis described above, isolating by
601 desired experimental context and radiation condition, and screening for sorted-cells only in the preinfected
602 case.
603 Differential gene expression analysis yielded log2 fold changes per gene per perturbation-context-radiation
604 condition. We constructed log2 fold change matrices the same way as the original differential gene analysis,
605 then used the RT and noRT condition gene modules from the non-downsampled non-negative matrix
606 factorization to collapse the corresponding downsampled log2 fold change matrices into matrices showing
607 module by perturbation. We also built a modified version of the non-downsampled log fold change matrix that
608 included only the perturbations used in the downsampled matrix.
609 We then calculated Pearson correlation between the collapsed downsampled matrix and the collapsed
610 non-downsampled matrix by comparing log2 fold changes by perturbation across the modules (the compared

vectors being a perturbation's averaged LFCs per module), as well as by module across the perturbations (the compared vectors being a module's averaged LFCs per perturbation across all experimental contexts).

Microenvironment perturb-seq analysis

Preprocessing, data transformation, and UMAP analysis was performed using Cell Ranger version 6.1.2 with sgRNA barcoding (10X Genomics) followed by Seurat version 4.3.0[11] in R version 4.3.1 as described above. For microenvironment cells, cells with greater than 200 but fewer than 5000 detected features were retained. Cells with greater than 25% mitochondrial RNA proportion were removed. Cell types were identified by performing Louvain clustering using the first 30 dimensions from PCA space and using a resolution parameter of 0.1. Top marker genes from these clusters were queried in EnrichR[17,18]. Unbiased cell type annotation was also performed using scMRMA as described above, with good agreement to cluster based annotations. SB28 cells were readily identified by overexpression of *Nras*[10]. On target gene knockdown analysis was performed as described above. For the microenvironment analysis differential gene expression analysis, we ran a condensed version of the differential expression and NMF methods from the malignant cell analysis described above. First, we filtered for only perturbations with more than 5 cells represented and only for cell types in which more than 5 cells expressed sgRNAs corresponding to the negative control sgnRNA. Next, we ran DESeq::findDE, using the cells with the negative control perturbation as the control group. We considered genes differentially expressed if they had a p-value < 0.05 and an absolute value log2 fold change > 0.1 for at least one of the perturbations.

Cell-cell interaction analysis between ligands and receptors was performed using CellChat version 1.6.1 [19], using the CellChatDB.mouse interaction database. Overexpressed genes and interactions were identified, and communication probability was determined using a truncatedMean approach with trim = 0.05, a minimum of 10 cells per communication, with weighting of relative population size. Differentially expressed genes from perturb-seq analysis were overlapped with significant source or target ligand-receptor pairs and visualized as dotplots. To calculate statistical significance for differences in cell-cell interactions between perturbed and control cells, two tailed Student's t tests were performed on the distribution of communication probabilities between a given ligand (for source cells) or receptor (for target cells) and their predicted interaction partners outputted by CellChat.

Online Methods References

1. Gilbert, L. A. *et al.* Genome-Scale CRISPR-Mediated Control of Gene Repression and Activation. *Cell* **159**, 647–661 (2014).

2. Gilbert, L. A. *et al.* CRISPR-mediated modular RNA-guided regulation of transcription in eukaryotes. *Cell* **154**, 442–451 (2013).

3. Horlbeck, M. A. *et al.* Compact and highly active next-generation libraries for CRISPR-mediated gene repression and activation. *eLife* **5**, 914 (2016).

4. Replogle, J. M. *et al.* Maximizing CRISPRi efficacy and accessibility with dual-sgRNA libraries and optimal effectors. *eLife* **11**, e81856 (2022).

5. Ozawa, T. & James, C. D. Establishing Intracranial Brain Tumor Xenografts With Subsequent Analysis of Tumor Growth and Response to Therapy using Bioluminescence Imaging. *J. Vis. Exp. : JoVE* 1986 (2010) doi:10.3791/1986.

6. Chen, P.-Y. *et al.* Comparing routes of delivery for nanoliposomal irinotecan shows superior anti-tumor activity of local administration in treating intracranial glioblastoma xenografts. *Neuro-Oncol.* **15**, 189–197 (2013).

659 7. Serwer, L., Hashizume, R., Ozawa, T. & James, C. D. Systemic and Local Drug Delivery for Treating
660 Diseases of the Central Nervous System in Rodent Models. *J. Vis. Exp. : JoVE* 1992 (2010)
661 doi:10.3791/1992.

662 8. Ozawa, T. *et al.* Response of intracerebral human glioblastoma xenografts to multifraction radiation
663 exposures. *Int. J. Radiat. Oncol.Biol.Phys.* **66**, 263–270 (2006).

664 9. Replogle, J. M. *et al.* Combinatorial single-cell CRISPR screens by direct guide RNA capture and targeted
665 sequencing. *Nature Biotechnology* **38**, 954–961 (2020).

666 10. Kosaka, A., Ohkuri, T. & Okada, H. Combination of an agonistic anti-CD40 monoclonal antibody and the
667 COX-2 inhibitor celecoxib induces anti-glioma effects by promotion of type-1 immunity in myeloid cells and T-
668 cells. *Cancer Immunol Immunother* **63**, 847–857 (2014).

669 11. Stuart, T. *et al.* Comprehensive Integration of Single-Cell Data. *Cell* **177**, 1888-1902.e21 (2019).

670 12. Hafemeister, C. & Satija, R. Normalization and variance stabilization of single-cell RNA-seq data using
671 regularized negative binomial regression. *Genome Biol.* **20**, 296 (2019).

672 13. Li, J., Sheng, Q., Shyr, Y. & Liu, Q. scMRMA: single cell multiresolution marker-based annotation. *Nucleic*
673 *Acids Res* **50**, gkab931- (2021).

674 14. Franzén, O., Gan, L.-M. & Björkegren, J. L. M. PanglaoDB: a web server for exploration of mouse and
675 human single-cell RNA sequencing data. *Database* **2019**, baz046 (2019).

676 15. Blanco-Carmona, E. Generating publication ready visualizations for Single Cell transcriptomics using
677 SCpubr. *bioRxiv* 2022.02.28.482303 (2022) doi:10.1101/2022.02.28.482303.

678 16. Hafemeister, C. & Halbritter, F. Single-cell RNA-seq differential expression tests within a sample should
679 use pseudo-bulk data of pseudo-replicates. *bioRxiv* 2023.03.28.534443 (2023)
680 doi:10.1101/2023.03.28.534443.

681 17. Kuleshov, M. V. *et al.* Enrichr: a comprehensive gene set enrichment analysis web server 2016 update.
682 *Nucleic acids research* **44**, W90-7 (2016).

683 18. Chen, E. Y. *et al.* Enrichr: interactive and collaborative HTML5 gene list enrichment analysis tool. *BMC*
684 *bioinformatics* **14**, 128 (2013).

685 19. Jin, S. *et al.* Inference and analysis of cell-cell communication using CellChat. *Nat Commun* **12**, 1088
686 (2021).

687
688